Dalton Transactions

Accepted Manuscript

Cite this: DOI: 10.1039/c0xx00000x

www.rsc.org/xxxxxx

ARTICLE TYPE

α $MnMoO_4$/Graphene Hybrid Composite: High Energy Density Supercapacitor Electrode Material

*Debasis Ghosh,[1] Soumen Giri,[1] Md. Moniruzzaman,[2] Tanya Basu,[2] Manas Mandal,[1] Chapal Kumar Das[1]**

Received (in XXX, XXX) Xth XXXXXXXXX 20XX, Accepted Xth XXXXXXXXX 20XX

DOI: 10.1039/b000000x

A unique and cost effective hydrothermal procedure has been carried out for the synthesis of hexahedron shaped α $MnMoO_4$ and its hybrid composite with graphene using three different weight percentage of graphene. Characterization techniques, such as, XRD, Raman and FTIR analysis established the phase and formation of the composite. The electrochemical characterization of the pseudocapacitive $MnMoO_4$ and the $MnMoO_4$ /graphene composites in 1 M Na_2SO_4 displayed highest specific capacitance of 234 F/g and 364 F/g, respectively at current density of 2 A/g. Unlike many other pseudocapacitive electrode materials our prepared materials responded with a wide range of working potential of (–) 1 V to (+) 1 V, which indeed resulted in high energy density without substantial loss of power density. The highest energy density of 130 Wh/kg and 202.2 Wh/kg was achieved, respectively for the $MnMoO_4$ and the $MnMoO_4$/graphene composite at a constant power delivery rate of 2000 W/kg. The synergistic effect of the graphene with pseudocapacitive $MnMoO_4$ caused an increased cycle stability of 88% specific capacitance retention after1000 consecutive charge discharge cycles at 8 A/g constant current density, which was higher than the virgin $MnMoO_4$ with 84% specific capacitance retention.

Introduction

Supercapacitor has attracted the new generation energy research with its unique properties of instant power supply with high energy density and long term cyclic stability and finds application in memory back up, hybrid electric vehicles, medical, military, aerial lift, public transport buses, etc. Supercapacitor, the eco-friendly energy resource has minimized the limitations of the other two conventional energy sources, the rechargeable battery and the capacitor in terms of both high power density and high energy density. The very high amount of charge stored in supercapacitor can be considered as individual or combined contribution of the electron transfer faradaic reaction (pseudocapacitance), and the electrical double layer formation by the electrostatic interaction between the oppositely charged ions at the electrode material/electrolyte interface (electrical double layer capacitance (EDLC)).[1] The total amount of charge stored in pseudocapacitor is many times higher than the EDLCs, however, shrinking or swelling is a major problem with these electroactive materials, which reduces their cycle life during consecutive charging and discharging. Use of electroactive materials with carbonaceous materials can respond unexpectedly good owing to a good synergistic between the two. Electroactive materials like $Ni(OH)_2$, $Co(OH)_2$, MnO_2, SnO_2, Co_3O_4, etc. have been widely investigated as pseudocapacitive electrode material stand alone,[2-6] or with combination of high surface area carbonaceous materials such as, activated carbon, CNT, graphene, etc.[7-11] In recent years mixed metal oxides have attracted severe attention due to their variable oxidation states, which leads to feasible electron transfer redox reaction in suitable electrolyte. $AMoO_4$ (A= Ni, Co, Mn, etc.) is a new class of mixed metal oxide, the investigation of which as supercapacitor electrode material is in primary level. Amongst the pseudocapacitive mixed metal oxides $NiMoO_4$ has been found to show the maximum specific capacitance of 1517 F/g and energy density of 52.7 Wh/Kg at a current density of 1.2 A/g.[12] Liu et al have achieved specific capacitance of 326 F/g for the $CoMoO_4$, 0.9 H_2O nanorods at a current density of 5 mA cm^{-2}.[13] On the other hand Mai et al have reported high specific capacitance of 204.1 F/g with energy density of 28.4 Wh/kg for the heterostructured, nanowires of $MnMoO_4$/$CoMoO_4$ at 0.5 A/g current density.[14] Xie et al obtained an improved specific capacitance of 394.5 F/g for the $CoMoO_4$/graphene composite at 1 mV/s scan rate.[15] Although the measured specific capacitances were considerably high for all of above reported materials/composites, the low working potential restricts their energy density, which is the key requirement for the excellence. The available commercial supercapacitors are mainly based on carbonaceous material with high surface area having energy density of 3-4 Wh/kg and power density of 3-4 kW/kg. However, the lack of sufficient energy density and power density often limits their applications in case of hybrid vehicles and automobiles.[16] It's a general concept that the output energy density and power density of supercapacitor electrode are closely related to their working potential. High energy density often causes significant loss of power density. So the challenge is to improve the energy density of supercapacitor electrode material without significant loss of power density and cycle stability.

In our present work we have prepared hexahedron shaped $MnMoO_4$ by the simple and cost effective hydrothermal process using easily available precursors. Hydrothermal procedure is a cost effective and the simplest procedure for the large scale synthesis of water insoluble metal oxides with high purity and controllable morphology using water soluble metal precursors at high pressure and moderated temperature. One benefit of this procedure is that it avoids the use of any hazards catalysts, seeds, injurious surfactants or template and is environmental benign. The presence of multiple redox active functionality in the $MnMoO_4$ enables its high pseudocapacitance. The ability to sweep within a large potential of 2 V in aqueous Na_2SO_4 electrolyte facilitates its high energy density at a high power delivery rate. However, the low conductance of the metal oxide restricts the current response and may not supply the expected energy density at high power density; hence improvement of conductance is still encouraged. To address this issue we have also synthesized graphene based hybrid composites of the pseudocapacitive $MnMoO_4$ using different weight percentage of exfoliated graphene. Graphene is the unique carbonaceous material with sp^2 hybridized carbon atoms arranged in a honey comb fashion exhibiting highest specific surface area and conductivity amongst all carbonaceous materials. Apart from that it can also act as an EDLC source, stand alone. The hybrid composites responded with increased specific capacitance, cycle stability as well as improved energy density. The various weight percentage of graphene was used to get the proper composition of the hybrid composite for obtaining the best electrochemical results.

Preparation of material

Exfoliated graphene was synthesized from natural graphite by a gum arabic assisted physical sonication followed by nitric acid treatment.[17] Analytical grade 20 ml 0.1 M $MnCl_2$ solution was thoroughly mixed with 20 ml 0.1 M Na_2MoO_4 solution with continuous stirring and the resulting solution was placed in a 50 ml Teflon sealed autoclave and maintained at 180°C for 15h. In another beaker the as prepared graphene powder was well dispersed in a mixture of 20 ml 0.1 M $MnCl_2$ solution and 20 ml 0.1 M Na_2MoO_4 solution via ultrasonication for 1h. Then the whole mixture was transferred to another teflon sealed autoclave with 50 ml capacity and maintained at 180°C for 15h. The resulting materials were washed with 2% ethanol in distilled water several times and dried at 60°C and collected. We used the graphene (Gr) powder in three different weight of 15 mg, 30 mg and 45 mg, and from the total weight of the Gr-$MnMoO_4$ composite it was found that the % of graphene in the composites were 3.1%, 6.7% and 10.4%, respectively. The as prepared materials were leveled as $MnMoO_4$, Gr-$MnMoO_4$ (I), Gr-$MnMoO_4$ (II) and Gr-$MnMoO_4$ (III), respectively.

Morphological analysis

Fig. 1a and 1b represents the FESEM images of the as prepared $MnMoO_4$ revealing its asymmetric hexahedron like morphology. In Fig. 1b the EDX mapping of the single crystal of $MnMoO_4$ clearly proves the presence of Mn, Mo and O. Fig. 1c, 1d and Fig. 1e represents the FESEM images of the Gr-$MnMoO_4$ (I), Gr-$MnMoO_4$ (II) and Gr-$MnMoO_4$ (III), respectively. In case of the Gr-$MnMoO_4$ (II), the $MnMoO_4$ crystals are well covered by the graphene sheets (more SEM image of $MnMoO_4$ and Gr-$MnMoO_4$ (II) is shown in ESI). Some bare $MnMoO_4$ crystals can be seen in Fig. 1c, whereas, a higher percentage of graphene leads to restacking of the graphene sheets, as shown in Fig. 1e. The TEM image of the $MnMoO_4$ also strengthens the asymmetric hexahedron morphology, as obtained from FESEM analysis. The SAED pattern of the $MnMoO_4$ (Fig. 1i) confirms its single crystalline nature. Fig. 1g represents the TEM image one of the Gr-$MnMoO_4$ (here Gr-$MnMoO_4$ (II)) composite indicating the

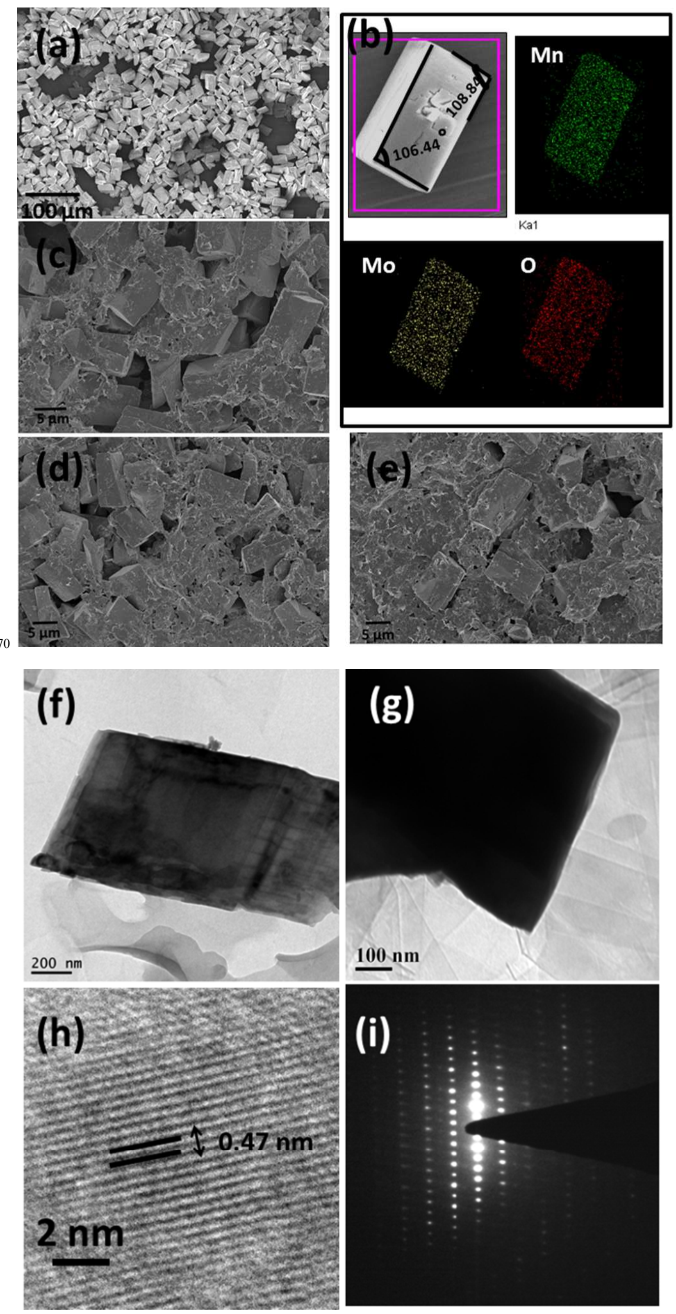

Fig. 1 The FESEM image of as prepared (a) $MnMoO_4$ hexahedrons, (b) EDX mapping of a hexahedron $MnMoO_4$ single crystal, SEM image of (c) Gr-$MnMoO_4$ (I), (d) Gr-$MnMoO_4$ (II), (e) Gr-$MnMoO_4$ (III); TEM

images of (f) $MnMoO_4$, (g) Gr-$MnMoO_4$ (II), (h) lattice fringes and (i) SAED pattern of the $MnMoO_4$ crystal.

distribution of the single crystal $MnMoO_4$ over exfoliated graphene. The lattice fringes of the single crystalline $MnMoO_4$ (Fig. 1h) are separated by a distance 0.47 nm indicating the crystalline growth of the single crystalline $MnMoO_4$ along the {-110} plane, which is also the highest intensity peak obtained from the XRD results (Fig. 2).

XRD pattern

Fig. 2 displays the XRD pattern of the as prepared pristine graphene, $MnMoO_4$, and Gr-$MnMoO_4$ (II). The crystalline peak at 26.4° in the XRD pattern of the as prepared pristine exfoliated graphene can be indexed to the (002) plane of hexagonal graphite (JCPDS card no. 41-1487). The XRD pattern of the hexahedron $MnMoO_4$ strongly resembles to the JCPDS file 78-0220 indicating the formation of manganese molybdenum oxide hydrate with anorthic crystal system having P-1 space group and chemical formula $Mn(MoO_4)$ (H_2O). The absence of any other peaks confirms the phase purity of the as prepared $MnMoO_4$. In case of the $MnMoO_4$ the crystalline peak at 2θ=26.41° can be indexed as {-1-11} plane (PDF card no. 78-0220). Again for exfoliated graphene the crystalline plane appears at 2θ= 26.4° and can be indexed as {002} plane. So the peak corresponding to {-1-11} of $MnMoO_4$ and {002} plane of exfoliated graphene fall in same location at 2θ= 26.4°. So it can be concluded that the peak at 2θ= 26.4° in the binary composite Gr-$MnMoO_4$ (II) comes from both the plane.

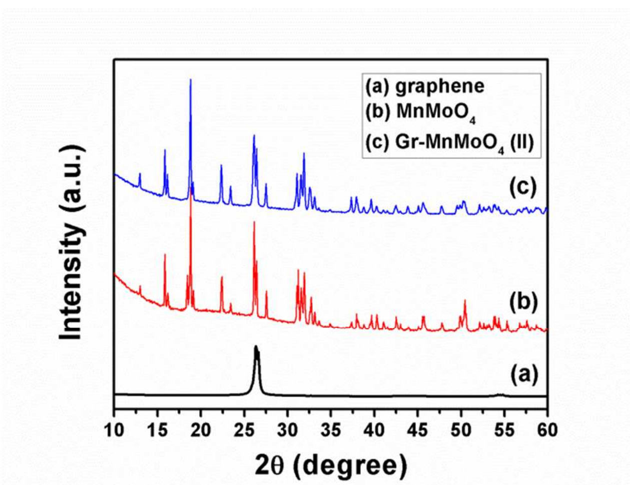

Fig. 2 XRD pattern of as prepared pristine graphene, $MnMoO_4$ and Gr-$MnMoO_4$ (II).

Raman analysis

The structure of the as prepared $MnMoO_4$ and Gr-$MnMoO_4$ (II) was also studied by Raman spectroscopy and the spectra are shown in Fig. 3. The spectrum of the as prepared $MnMoO_4$ exhibits sharp line at 926 cm^{-1}, medium intense lines at 862 cm^{-1}, 328 cm^{-1}, and low intense line at 820 cm^{-1}, 796 cm^{-1} and 363 cm^{-1}. These are the characteristic bands of $MnMoO_4$.[14] In the graphene based hybrid composite of α $MnMoO_4$ along with all the red shifted peaks of $MnMoO_4$ some extra peaks appear at 1340 cm^{-1}, 1580 cm^{-1} and 2682 cm^{-1}, corresponding to the disordered induced D band, G band and the 2D band of graphene, respectively.[18] The D band represents the disorder induced in the graphitic structure, whereas the G band appears from the vibration of sp^2-bonded carbon atoms and is corresponded to the E2g mode of graphite.[19] The intensity ratio of the D band and G band determines the defect in the graphitic structure. A small defect ratio (I_d/I_g) of 0.25 was derived for the exfoliated graphene in the Gr-$MnMoO_4$ (II) composite indicating a few basal plane defects and only moderate levels of edge defects.[12] The 2D band is the second order D band and is also called the overtone of the D band and is also a Raman signature of graphitic sp^2-bonded carbon atoms. For single layer graphene the 2D band should be sharp, however, the broad 2D band in the Gr-$MnMoO_4$ (II) composite indicates a few layered graphene.[20] In the Gr-$MnMoO_4$ (II) composite the red shifting of the $MnMoO_4$ bands is a signature of the fact that the graphene does not just act as a basal plane for the crystalline $MnMoO_4$ rather establishes some sort of chemical interactions between the two. The interaction of the graphene with the metal molybdate is possibly through both chemical covalent bonding at the oxygen-containing sites and van der Waals interaction with conjugated domains of graphene.[21]

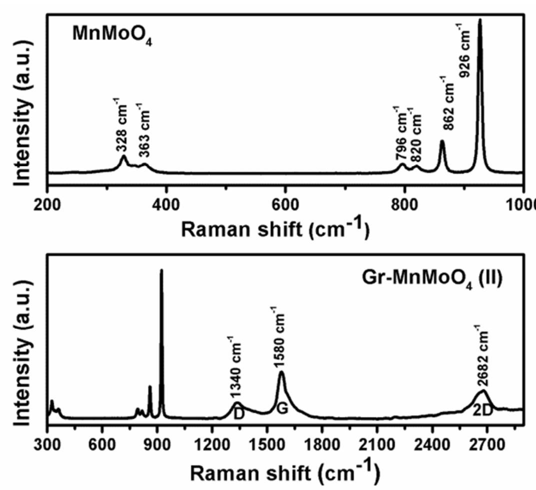

Fig. 3 Raman spectra of the as prepared $MnMoO_4$ and Gr-$MnMoO_4$ (II).

FTIR analysis

Both the $MnMoO_4$ and Gr-$MnMoO_4$ (II) exhibited similar FTIR plots (Fig. 4) with intense peaks at 715, 785, 896, and 941 cm^{-1}. These peaks are the characteristic peaks of α phase of $MnMoO_4$, where the central metal atom Mo has the tetrahedral coordination at the surface.[22] The peak at 941 cm^{-1} can be attributed to the Mo=O groups stretching frequency.[21] The peak at 896 cm^{-1} can be assigned to the of Mo–O–Mo bending vibration.[23] The other two peaks around 1617 cm^{-1} and 3434 cm^{-1} can be attributed to the O-H stretching and H-OH bending vibration of the surface adsorbed water molecules.

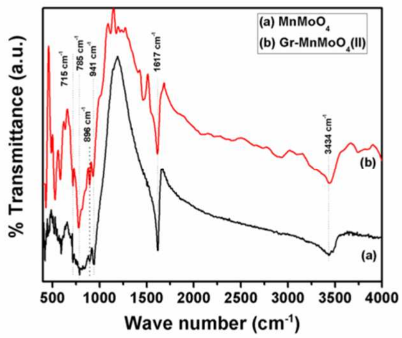

Fig. 4 FTIR plot of $MnMoO_4$ and Gr-$MnMoO_4$ (II).

BET analysis

The Bruauer–Emmet–Teller (BET) analysis was performed for both the $MnMoO_4$ and Gr-$MnMoO_4$ (II) in order to understand the specific surface area and pore size distribution of the materials. Fig. 5a and 5c represents the N_2 adsorption/desorption isotherm at 77.3 K of the $MnMoO_4$ and Gr-$MnMoO_4$ (II), respectively. Both the isotherms are of Type-IV with a hysteresis loop, attributed to the abundance of mesopores inside the material. The BET surface area of the $MnMoO_4$ was calculated to be 5.77 m^2/gm, which was higher than that of $MnMoO_4$ nanorod with BET surface area of 3.17m^2/gm.[14] The added graphene with a percentage of 6.7% increase the surface area of the Gr-$MnMoO_4$ (II) composite to 8.78 m^2/gm. Fig. 5b and 5d represents the pore size distribution plot of $MnMoO_4$ and Gr-$MnMoO_4$ (II), respectively.

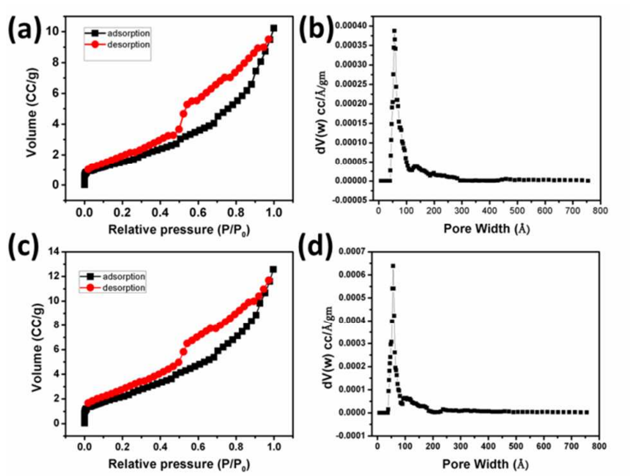

Fig. 5 N_2 sorption isotherms of (a) $MnMoO_4$ and (c) Gr-$MnMoO_4$ (II); pore size distribution of (b) $MnMoO_4$ and (d) Gr-$MnMoO_4$ (II).

Both the materials showed predominant mesopores (2-50 nm) with a sharp peak around 5.68 nm and it was sharper in case of Gr-$MnMoO_4$ (II). The mesoporous structures are well accessible by the electrolyte ions, leading to fast rate of charge transfer. The total pore volume of 1.582e^{-02} cc/g was calculated from the DFT method for 0.1465 g $MnMoO_4$ for pores smaller than 13097.8 Å (diameter) at P/P_o of 0.99645. For the Gr-$MnMoO_4$ (II) composite with 0.1455 g material a total pore volume of 1.950e^{-02} cc/g was calculated for pores smaller than 5416.1 Å (diameter) at P/P_o of 0.99645.

Electrochemical characterizations

The electrochemical performances of the as prepared $MnMoO_4$ and its graphene based hybrid composites were studied by a three electrode system. 1.5% nafion solution in ethanol was used as a binder. Nafion as a binder can influence the electrochemical performances of the electrode materials. Lufrano et al[24] established that 10-30% nafion as binder has a very little effect on specific capacitance; hence it can be considered that 1.5% nafion would have negligible effect on the electrochemical performances of the electrode materials.[25] Cyclic Voltammetry (CV), galvanostatic charge discharge (GCD) and electrochemical impedance spectroscopy (EIS) were executed to analyze the electrode performances and the electrolyte used was 1M Na_2SO_4. The specific capacitance of the materials from the CV experiment was calculated by using the following equation,

$$\text{Specific capacitance } (C_s) = \frac{\int_{v1}^{v2} i\,(v)dv}{(v2-v1)\,vm}$$

In the equation, the numerator calculates the area under the CV curve, V_1 and V_2 are the two potential limits, ν is the scan rate and m is the electrode mass.

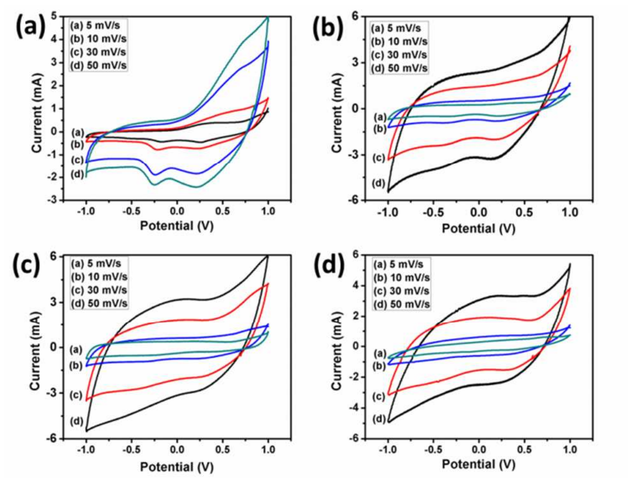

Fig.6 CV plots of (a) $MnMoO_4$, (b) Gr-$MnMoO_4$ (I), (c) Gr-$MnMoO_4$ (II) and (d) Gr-$MnMoO_4$ (III) at different scan rates of 5 mV/s, 10 mV/s, 30 mV/s and 50 mV/s.

Fig. 6a represents the CV plots of $MnMoO_4$ with in the potential range of (–) 1 V to (+) 1 V at various scan rates of 5 mV/s, 10 mV/s, 30 mV/s and 50 mV/s. The highest specific capacitance obtained from the $MnMoO_4$ electrode was 267 F/g at a scan rate of 5 mV/s. A couple of redox peak can be observed in the CV plots of $MnMoO_4$ indicating its redox activity. The redox peaks are associated with the reversible electron transfer between the Mn (II) and Mn (III) state. The redox peak potential shows a positive shift for the cathodic peaks and a negative shift for the anodic peaks with the increasing scan rate, which may be due to the various resistive effect involved with the electrode. Again the increasing peak current with increasing scan rate is a consequence of the diffusion controlled process.[26] The well resolved redox peaks can be observed even at high scan rate of 50 mV/s and the redox peaks were reproducible, which also signify excellent rate capability of the electrode material.[12] Although aqueous electrolyte tends to decompose beyond 1.23 V, the as prepared

$MnMoO_4$ shows a high operation voltage close to 2 V. The probable explanation is the overpotential, where oxygen evolution from water does not follow a measurable rate until extra potentials is reached.[27] There is an increase in peak current near +1 V, possibly due to the oxygen evolution at the electrode. In case of the negative potential window, the current response does not increase as the negative cut off potential (–1 V) is reached, possibly due to the overpotential for hydrogen evolution at the $MnMoO_4$ electrode.[28] The redox reaction can be represented as

$MnMoO_4 + Na^+ + e^- \leftrightarrow NaMnMoO_4$

The obtained specific capacitance of $MnMoO_4$ is mainly directed by the above redox reaction. Mo atom does not take part directly in any faradaic process, hence almost no input towards pseudocapacitance. However, the incorporation of Mo results in increased conductivity of $MnMoO_4$ to 4.27 e^{-3} S/cm (fig. 8), which indeed helps to achieve the enhanced electrochemical capacitance.[14, 29-30] We investigated the electrode performance of the graphene based hybrid composite of $MnMoO_4$ with in the same potential range to that of $MnMoO_4$. To verify the effect of graphene we performed the CV test for all Gr-$MnMoO_4$ (I), Gr-$MnMoO_4$ (II) and Gr-$MnMoO_4$ (III) composites at different scan rates of 5 mV/s, 10 mV/s, 30 mV/s and 50 mV/s and the respective CV plots are shown in Fig. 6b, 6c and 6d. The scan rate dependent specific capacitances of the $MnMoO_4$ and all its graphene based composites are shown in Table 1. The highest specific capacitance obtained for the Gr-$MnMoO_4$ (I), Gr-$MnMoO_4$ (II) and Gr-$MnMoO_4$ (III) was 375 F/g, 395 F/g and 354 F/g, respectively at 5 mV/s scan rate. With the increasing amount of graphene from 3.1% to 6.7% in the composites the specific capacitance also increased. However, composite with the highest amount of graphene (10.4 %) showed lowest specific capacitance; hence the CV results indicate that the majority of the specific capacitance contribution comes from the pseudocapacitive $MnMoO_4$ and also a better synergistic effect between graphene and $MnMoO_4$ with the 6.7% graphene loading.

Table 1. Various specific capacitances obtained for the $MnMoO_4$, Gr-$MnMoO_4$ (I), Gr-$MnMoO_4$ (II) and Gr-$MnMoO_4$ (III) composite at different scan rate.

Scan rate (mV/s)	5	10	30	50
SC of $MnMoO_4$ (F/g)	267	234	209	174
SC of Gr-$MnMoO_4$ (I) (F/g)	375	338	317	292
SC of Gr-$MnMoO_4$ (II) (F/g)	395	354	336	316
SC of Gr-$MnMoO_4$ (III) (F/g)	354	316	293	272

The symmetrical nature of the CV plots and the close mirror image current response on voltage reversal of all the Gr-$MnMoO_4$ composites indicate their comparative ideal supercapacitive behavior. In the CV plot of $MnMoO_4$, the reduction peak is more prominent than the oxidation peak indicating a quasi-reversible redox process. Interaction of highly conductive and high surface area graphene with the $MnMoO_4$ crystal increases the conductivity, surface area and porosity of the composite. The increased surface area also increases the contact area of the composite electrode with the electrolyte assuring that plenty of electrolyte ions can come in contact; at the same time increased conductivity leads to the easy ion transport thus maintaining excellent reversibility. Interesting to observe that as the graphene content increases the peak intensity decreases and a more flat CV plot was obtained. The diminishing of the redox peaks with increasing graphene content indicates that the composite electrode material with higher graphene content are charged and discharged at a pseudo-constant rate over the entire voltammetry cycles, where the total specific capacitance can be considered as the redox capacitance of $MnMoO_4$ combined with the double layer capacitance of graphene.[31] The specific capacitance value gradually decreases with increasing scan rate, a consequence of time dependent faradaic reaction, which is slow enough to occur at high scan rate. The % of specific capacitance retention of the $MnMoO_4$, Gr-$MnMoO_4$ (I), Gr-$MnMoO_4$ (II) and Gr-$MnMoO_4$ (III) were 65.2%, 77.8%, 80%, 76.8%, respectively at high scan rate of 50 mV/s with respect to the low scan rate of 5 mV/s. The excellent current response from the CV plots for the $MnMoO_4$ and all of its graphene based composites indicates a rapid kinetics of the interfacial faradaic redox reactions and as well as high rates of electronic and ionic transport even at high scan rate of 50 mV/s.[13]

The galvanostatic charge discharge (GCD) of the as prepared $MnMoO_4$ and its graphene based composites were carried out at current density of 2A/g within the potential range of (–) 1 V to (+) 1 V and the comparative GCD plots are shown in Fig. 7a. The nonlinear GCD plot of the $MnMoO_4$ indicates its pseudocapacitive behavior. On the other hand the GCD plots of graphene based composites of $MnMoO_4$ shows comparative linear character indicating some ideal behavior. The specific capacitance from the GCD plots was calculated from the following equation

$$\text{Specific capacitance} = \frac{i \times \Delta t}{\Delta v \times m}$$

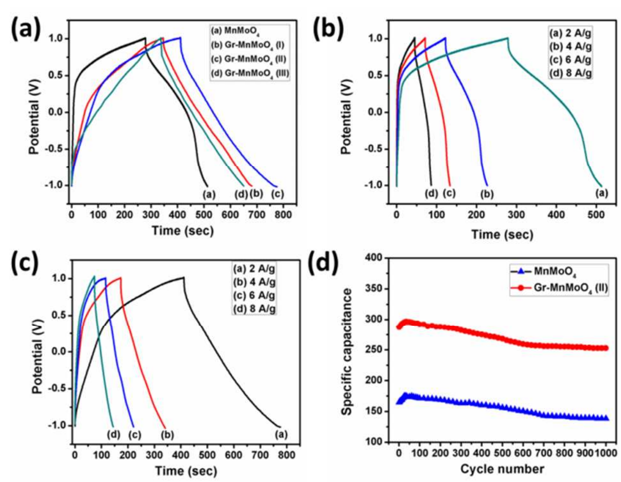

Fig. 7 (a) Comparative GCD plots of $MnMoO_4$, Gr-$MnMoO_4$ (I), Gr-$MnMoO_4$ (II) and Gr-$MnMoO_4$ (III) at constant current density of 2A/g; GCD plots of (b) $MnMoO_4$ and (c) Gr-$MnMoO_4$ (II) at different current density of 2 A/g, 4 A/g, 6 A/g and 8 A/g; (d) Variation of specific capacitance as a function of cycle number of the $MnMoO_4$ and Gr-$MnMoO_4$ at 8 A/g current density.

Where (i/m) is a measure of the current density, t is the discharge time and ΔV considers the potential window. The maximum specific

capacitance obtained from the $MnMoO_4$ electrode was 234 F/g at 2A/g current density. The high utility of the pseudocapacitive

$MnMoO_4$ as electrode material was achieved in its graphene based hybrid composites. A maximum specific capacitance of 364 F/g was obtained for the Gr-$MnMoO_4$ (II) composite at 2A/g current density, which was higher compared to that of both the Gr-$MnMoO_4$ (I) and Gr-$MnMoO_4$ (III), exhibiting specific capacitance of 336 F/g and 313 F/g, respectively. For better understanding the high current application of the electrode materials we performed the GCD test of the $MnMoO_4$ and Gr-$MnMoO_4$ (II) at different higher current densities of 4 A/g, 6 A/g and 8 A/g and the corresponding GCD plots are shown in Fig. 7b and Fig. 7c, respectively, and the calculated specific capacitances are shown in Table 2.

Table 2. Various specific capacitances obtained for $MnMoO_4$ and Gr-$MnMoO_4$ (II) composites at different current densities.

Current density (A/g)	2	4	6	8
SC of $MnMoO_4$ (F/g)	234	210	187	165
SC of Gr-$MnMoO_4$ (II) (F/g)	364	338	314	287

With the increasing current density the specific capacitance value shows a decreasing order, which is a consequence of the less availability of the active redox sites at high current density; however, still specific capacitance retention of 70.5% and 78.8%, respectively for $MnMoO_4$ and Gr-$MnMoO_4$ (II) at high current density of 8 A/g with respect to low current density of 2A/g signifies their excellent rate capability. The decreasing of specific capacitance with increasing current density is a consequence of the less availability of the electroactive site at high current. The cycle stability of the $MnMoO_4$ and Gr-$MnMoO_4$ (II) was examined by continuing the GCD cycle to 1000 cycles at constant current density of 8 A/g and specific capacitance retention of 84% and 88% was achieved, respectively. Inspired from the highest specific capacitance obtained from the Gr-$MnMoO_4$ (II) composite we carried out further GCD cycles only for the same. The last four GCD cycles are shown in Fig. S3 (see supporting information).The specific capacitance response as a function of cycle number is shown in Fig. 7d. Apart from the initial increase of specific capacitance, a consequence of the wetting effect, the specific capacitance value shows a linear drop with increasing cycle numbers, which also follow the general trend of specific capacitance decay with cycle number for supercapacitor. The linear drop of specific capacitance with cycle number is rather slow at the end cycles indicating excellent reversibility of the electrode material. In case of the Gr-$MnMoO_4$ (II) composite the flexible and conductive graphene plays a dual role. It increases the electrical conductivity of the composite electrode by forming an interconnected conductive network, as well as, leads to an increment in the cycle life by releasing the mechanical strain involved during the consecutive GCD cycles. The better synergistic interaction between the high surface area and highly conductive graphene with the pseudocapacitive $MnMoO_4$ leads to increase the overall specific capacitance and also the cycle stability of the Gr-$MnMoO_4$ (II) composite. The energy density and power density was calculated from the following equations

Energy density (E) = $\frac{1}{2} C \times \Delta V^2$ (3)

Power density (P) = E/T (4)

Where, C, ΔV, and T represents the specific capacitance, potential window, energy density and the discharge time. The maximum energy density of about 130, 186.7, 202.2 and 173.9 Wh/kg was obtained for the $MnMoO_4$, Gr-$MnMoO_4$ (I), Gr-$MnMoO_4$ (II) and Gr-$MnMoO_4$ (III) composite, respectively at the power delivery rate of 2000 W/kg. The $MnMoO_4$ and Gr-$MnMoO_4$ (II) also responded with high energy density of 91.7 Wh/kg and 159.4 Wh/kg at high power density of 8000 W/kg. The very high energy density without significant loss of power density is a key to consider them as smart supercapacitor electrode material. The variation of energy density as a function of power density for the $MnMoO_4$ and Gr-$MnMoO_4$ is shown in Fig. 8b.

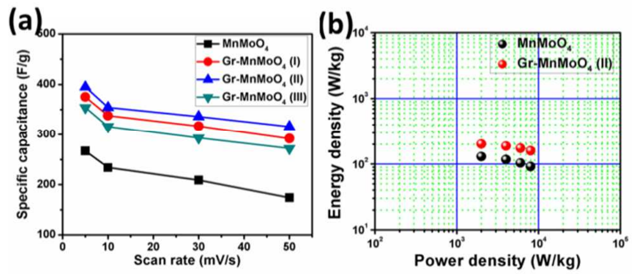

Fig. 8 (a) variation of specific capacitance as a function of scan rate of $MnMoO_4$, Gr-$MnMoO_4$ (I), Gr-$MnMoO_4$ (II) and Gr-$MnMoO_4$ (III), (b) plot of energy density as a function of power density of the $MnMoO_4$ and Gr-$MnMoO_4$ (II).

We also performed the EIS analysis of the $MnMoO_4$ and all of its graphene based hybrid composites within the frequency range of 1MHz to 1 mHz under the ac voltage amplitude of 10 mV. The EIS plots are represented in Fig. 9a in terms of Nyquist plots after fitting with an equivalent electrical circuit (Fig. 9b). Inset of Fig. 5a shows the expanded high frequency region of the same Nyquist plots. The Nyquist plots of all the materials exhibited similar nature starting with a depressed semicircle at the high frequency region followed by a line with approximate angle of 45° in the low frequency region. The initial semicircle indicates blocking behavior of the electrode materials at high frequency and the post semicircle line indicates capacitive behavior at the low frequency. The high frequency semicircle diameter determines the charge transfer resistance, whereas, the point of intersection of the depressed semicircle with the real impedance axis in the high frequency region calculates the solution resistance. The post semicircle line with an angle close to 45° indicates the Warburg behavior of the electrode material i.e. diffusion controlled doping and de-doping of the electrolyte ions. The extent of diffusion process is measured by the slope of the straight line at the low frequency region, and a line with higher slope indicates higher ion diffusion within the electrode material, hence corresponds to improved electrochemical behavior. The equivalent electrical circuit to which the Nyquist plots were fitted can be represented as $R_s+Q/(R_{ct}+W)+C_{dl}$, where the terms R_s, Q, R_{ct}, W and C_{dl} represents the solution resistance, constant phase element (CPE), charge transfer resistance, Warburg coefficient and the double layer capacitance, respectively. All the graphene based electrode materials exhibited similar solution resistance around 2.9-3 ohm, whereas a little higher solution resistance of 3.6 ohm

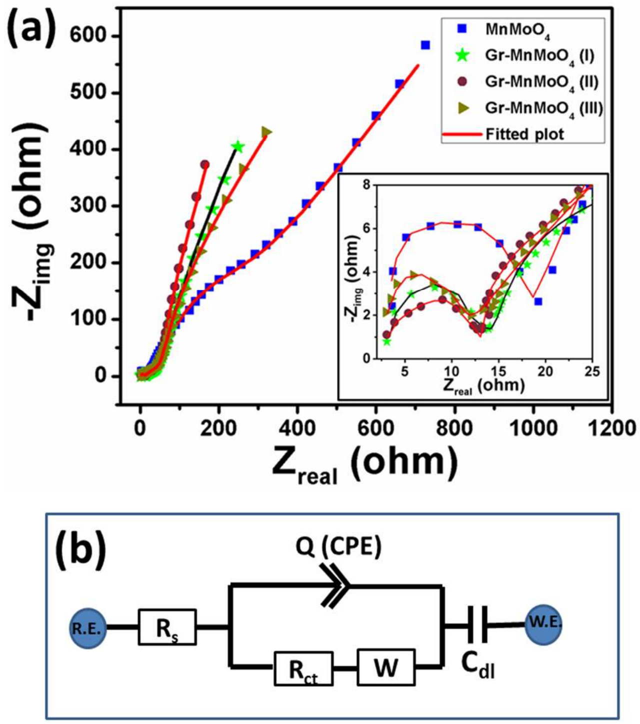

Fig 9. (a) Nyquist plots of $MnMoO_4$, Gr-$MnMoO_4$ (I), Gr-$MnMoO_4$ (II), Gr-$MnMoO_4$ (III) and the expanded high frequency plots are shown in inset, (b) the equivalent electrical circuit to which the Nyquist plots were fitted.

was observed for the $MnMoO_4$. The R_{ct} which measures the kinetics of the faradaic charge transfer reaction was calculated to be the highest for the $MnMoO_4$ and a gradual decreasing order was observed with increasing graphene content of the composites. The total equivalent series resistance of the porous electrode materials can be considered as the combined effect of the surface electrolyte resistance, electrolyte resistance inside the pore, electrode contact resistance, etc. For ideal capacitor the high frequency semicircle centre should be on the X axis and the low frequency straight line should be parallel to the imaginary impedance axis. However, the materials discussed presently do not follow it, which indicates deviation from perfect capacitor behavior of the electrode materials and is represented by the CPE. The CPE appears due to some physical defect inside the electrode material, i.e. different coating thickness at the current collector, rough electrode surface or the uneven reaction site distribution, etc. The CPE (Q) can be calculated by using the equation CPE = $1/(Z(\omega)\times(j\omega)^n)$. The frequency power n determines the ideal behaviour of the electrode material and for supercapacitor it varies as 0.5 □n □1. The n value closer to 1 indicates more ideal character. The n value was calculated to be 0.77, 0.82, 0.84 and 0.81 for the $MnMoO_4$, Gr-$MnMoO_4$ (I), Gr-$MnMoO_4$ (II) and Gr-$MnMoO_4$ (III), respectively. The various circuit parameters obtained from the fitted electrical circuit are shown in Table 3. We also performed the EIS analysis of the $MnMoO_4$ and Gr-$MnMoO_4$ after 1002 GCD cycles and the plots are shown in Fig. S3(see supporting information).

Table 3 various circuit parameters obtained from the fitted plot

	R_s (ohm)	R_{ct} (ohm)	C_{dl} (F)	W (ohm×$s^{-1/2}$)	Q (S×s^n)	n
$MnMoO_4$	3.6	15	2.1×10^{-6}	135.8×10^{-6}	2.3×10^{-6}	0.77
Gr- $MnMoO_4$ (I)	3.03	10.7	1.3	82.6×10^{-6}	3.4×10^{-6}	0.82
Gr- $MnMoO_4$ (II)	2.98	10	1.8	76×10^{-6}	4.2×10^{-6}	0.84
Gr- $MnMoO_4$ III)	2.88	9.2	2.1	61.9×10^{-6}	3.7×10^{-6}	0.81

The specific capacitance from the EIS was calculated by using the following equation

$$\text{Specific capacitance} = (-)\,1/(m\times\omega\times Z_{img}) \quad (5)$$

Where, m is the electrode mass, ω is the angular frequency and Z_{img} is the corresponding imaginary impedance. The specific capacitance of the as prepared $MnMoO_4$, Gr-$MnMoO_4$ (I), Gr-$MnMoO_4$ (II) and Gr-$MnMoO_4$ (III) was calculated to be 209 F/g, 311 F/g, 331 F/g and 286 F/g, respectively at low frequency of 3.23×10^{-3} Hz. The frequency dependent specific capacitance plot of the as prepared electrode materials is shown in Fig. 10. With the increasing frequency a rapid decrease of specific capacitance can be observed for all the materials indicating capacitive behavior at low frequency, resistor behavior at high frequency and a combination of capacitor and resistor behavior at the mid lower frequency. The specific capacitance obtained from the three different electrochemical measurements is different, as obvious from the different parameters involved with the measurements. The specific capacitance obtained from the CV and GCD experiment is a combination of both the differential capacitance and integral capacitance, whereas EIS measures only the differential capacitance. However, considering the device fabrication, the charge discharge result has more implications.

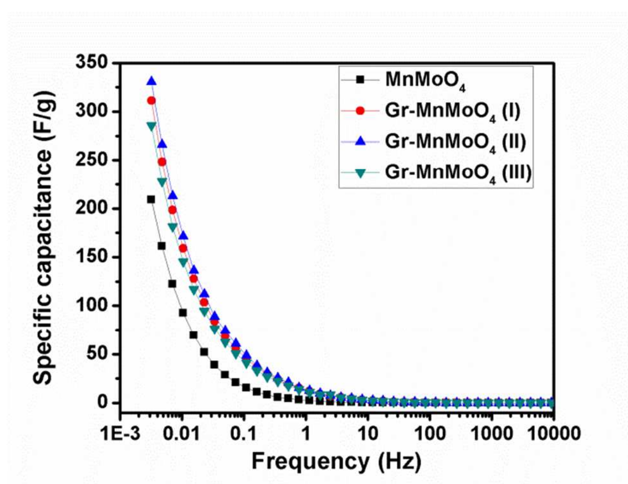

Fig. 10. Frequency dependent specific capacitance of $MnMoO_4$, Gr-$MnMoO_4$ (I), Gr-$MnMoO_4$ (II) and Gr-$MnMoO_4$ (III).

So from all the electrochemical characterizations, it can be stated that the high electrochemical utilization of the pseudocapacitive $MnMoO_4$ was achieved in its graphene based composite with 6.7% graphene loading. To validate the claim for device application the electrochemical measurements in terms of the CV and GCD were repeated for the $MnMoO_4$ and Gr-$MnMoO_4$(II) with high mass loading on Ni foam current collector, which closely resembles with that obtained with less mass loading in GC electrode (see supporting information Fig. S4). The electrical conductivity of the as prepared $MnMoO_4$ and Gr-$MnMoO_4$ (II) were further investigated.

Electrical measurement

The AC electrical conductivity of the as prepared pristine graphene, $MnMoO_4$ and Gr-$MnMoO_4$ (II) was carried out for the frequency ranging from 50 Hz to 10^6 Hz and the frequency dependent conductivity plot is shown in Fig.11. The nature of the plots in each case can be divided into two parts; initial low frequency response of conductivity is quite parallel to the frequency axis for both the materials followed by a sudden rise of conductivity in the high frequency region. The frequency at which the sudden increase in conductivity occurs is called the critical frequency (f_c).

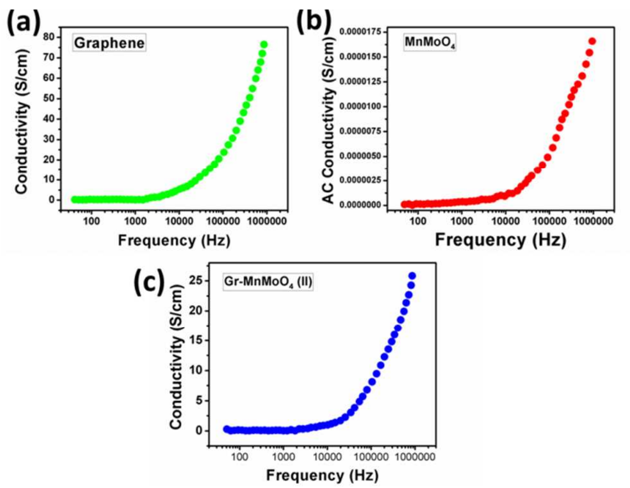

Fig. 11 Frequency dependent AC electrical conductivity of the (a) pristine graphene, (b) $MnMoO_4$ and (c) Gr-$MnMoO_4$ (II)

The relaxation phenomenon at low frequency plays a crucial role in the steady state of the conductivity. But at high frequency, the relaxation time is too short to maintain the orientation polarization of the dipole/induced dipole along the direction of applied electric field, which indeed results in increase in conductivity. The electrical conductivity of the $MnMoO_4$ is very low; however the Gr-$MnMoO_4$ composite exhibits reasonable high conductivity owing to the presence of highly conductive graphene. The interconnected network formed by graphene increases electron hoping and electron tunneling rate subsequently the conductivity increases.[32-33] The DC electrical conductivity of the as prepared graphene, $MnMoO_4$ and Gr-$MnMoO_4$ (II) composite was carried out using a four point probe method and the voltage response as a function of current is shown in Fig. 12. The conductivity was calculated using the following equation[34]

Conductivity (σ) $=1/\rho = 1/(\pi t/\ln 2(V/I)) = 1/(4.53\times t\times \text{resistance})$

Where t is the thickness in cm. The DC conductivity of 123 S/cm, $4.27e^{-3}$ S/cm and 19.43 S/cm was obtained for the pristine graphene, $MnMoO_4$ and Gr-$MnMoO_4$ (II), respectively. The electrical conductivity of MnO_2 is poor and is generally in the order 10^{-5}–10^{-6} S/cm.[4,35] Hence the high electrical conductivity of the mixed metal oxide $MnMoO_4$ over MnO_2 must be attributed to the presence of Mo.[29]

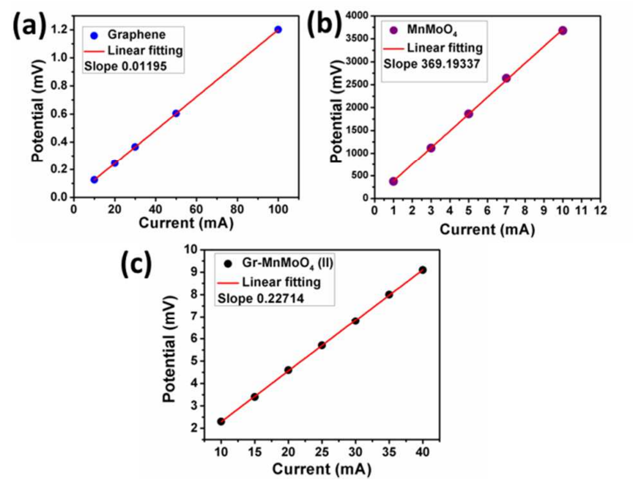

Fig.12 Plot of voltage response as a function of current for the measurement of DC electrical conductivity of Graphene, $MnMoO_4$ and Gr-$MnMoO_4$ (II).

Conclusion

Herein, we have reported improved electrochemical properties of the α $MnMoO_4$ in 1M Na_2SO_4 as supporting electrolyte. Due to the presence of various oxidation states of the metals forming $MnMoO_4$, it can act as pseudocapacitor. The compactness of the crystal structure results in achieving high electrochemical stability during consecutive GCD cycling. Unlike most other reported metal oxides, the prepared α $MnMoO_4$ is able to work under a large range of potential of (-) 1 V to (+) 1 V. The high value of pseudocapacitance and the large working potential help to achieve high energy density at a high power delivery rate. The high utility of the pseudocapacitive $MnMoO_4$ is achieved in its graphene based hybrid composite. Amongst the various weight percentages of graphene and $MnMoO_4$ the best electrochemical results can be obtained with 6.7 % weight of graphene. The wrapping of $MnMoO_4$ crystal by graphene having high surface area and high conductivity results in an excellent synergistic interaction between the two, which indeed increase the specific capacitance, energy density and reversibility of the composite electrode material. The highest energy density of 202.2 Wh/kg was achieved for the Gr-$MnMoO_4$ (II) composite at a steady power delivery rate of 2000 W/kg, which was higher than that of virgin $MnMoO_4$ exhibiting highest energy density of 130 Wh/kg at the same power density. The very high energy density without any significant loss of power density and the excellent cycle stability have enabled the Gr-$MnMoO_4$ (II) as superior electrode material for supercapacitor application.

Acknowledgement

We are thankful to the UGC, India, for the financial support and IIT Kharagpur for the instrumental help.

Notes

[1]*Materials Science Centre, Indian Institute of Technology Kharagpur, Kharagpur 721302, India.*

[2]School of Mechanical and Aerospace Engineering, Nanyang Technological University, Singapore
E-mail: chapal12@yahoo.co.in

†Electronic supplementary information (ESI) available: Description of materials used, instruments for characterizations, SEM image of $MnMoO_4$ and Gr-$MnMoO_4$ (II), TG-DTA analysis of $MnMoO_4$ and Gr-$MnMoO_4$ (II), last four GCD cycles (998-1002) and EIS in terms of Nyquist plot after GCD cycles of $MnMoO_4$ and Gr-$MnMoO_4$ (II). CV and GCD test of $MnMoO_4$ and Gr-$MnMoO_4$ (II) with high mass loading using Ni foam current collector.
See DOI: 10.1039/b000000x/

References

1 B. Conway, Kluwer Academic/Plenum Publishers, New York, 2nd ed, 1999.
2 G. S. Gund, D. P. Dubal, S. S. Shinde, C. D. Lokhande, *Ceram. Int.,* 2013, **39**,7255.
3 C. Mondal, M. Ganguly, P. K. Manna , S. M. Yusuf , T. Pal, *Langmuir*, 2013, **29**, 9179.
4 Z. Yu, B. Duong, D. Abbitt, J. Thomas, *Adv. Mat.* 2013, **25**, 3302.
5 S. Mijayakumar, S. Nagamuthu, K. K. Purushothaman, M. Dhanashankar, G. Muralidharan, *Int. J. Nanosci.,* 2011, **10**, 1245.
6 D. Ghosh, S. Giri, C. K. Das, *Environ. Prog. Sustain. Energy, DOI: 10.1002/ep.11874*
7 D. Ghosh, S. Giri, A. Mandal, C.K. Das, *Chem. Phys. Lett.,* 2013, **573,** 41.
8 D. Ghosh, S. Giri, C.K. Das, *ACS Sustainable Chem. Eng.*, 2013, **1,** 1135.
9 S. Chen , J. Zhu, X. Wu , Q. Han, Xin Wang, *ACS Nano*, 2010, **4,** 2822.
10 S.P. Lim, N.M. Huang, H.N. Lim, *Ceram. Int.*, 2013, **39,** 6647.
11 X –C. Dong, H. Xu, X- W. Wang, Y-X. Huang, B. C-P. Mary, H. Zhang, L-H.Wang, W. Huang, P. Chen, *ACS Nano,* 2012, **6**, 3206.
12 B. Senthilkumar, K. V. Sankar, R. K. Selvan, M. Danielle, M. Manickam, *RSC Adv.*, 2013, **3**, 352.
13 M-Cheng Liu, L-Bin Kong, X-Jing Ma, C. Lu, X-Ming Li, Y-Chun Luo, L. Kang, *New J. Chem.,* 2012, **36**, 1713.
14 L-Q. Mai, F. Yang, Y-L. Zhao, X. Xu, L. Xu, Y-Z Luo, *Nature Commun.*, 2011, **2**, 381.
15 X. Xia, W. Lei, Q. Hao, W. Wang and X. Wang, Electrochim. Acta, 2013, **99**, 253.
16 P.-C. Chen , G. Shen , Y. Shi , H. Chen, Chongwu Zhou, *ACS Nano*, 2010, **4**, 4403.
17 V. Chabot, B. Kim, B. Sloper, C. Tzoganakis and Aiping Yu, *Sci. Rep.*, 2013, **3**, 1378.
18 A. K. Gupta, C. Nisoli, P. E. Lammert, V. H. Crespi, P. C. Eklund, *J. Phys.: Condens. Matter*, 2010, **22**, 334205.
19 X. Fu, X. Song, Y. Zhang, *Mater. Lett.*, 2012, **70**, 181.
20 M. A. Pimenta, G. Dresselhaus, M. S. Dresselhaus, L. A.Cancado, A. Jorio, R. Sato, *Phys. Chem. Chem. Phys.*, 2007, **9**, 1276.
21 Y. Xu, X. Huang, Z. Lin, X. Zhong, Y. Huang, X. Duan, *Nano Res.* 2013, **6**, 65–76.
22 S. Lei, K. Tang, Q. Liu, Z. Fang, Q. Yang. H. Zheng, *J. Mater Sci,* 2006, **41**, 4737.
23 L. Seguin, M. Figlarz, R. Cavagnat, J.-C. Lasskgues, *Spectrochim. Acta A*, 1995, **51**, 1323.
24 F.Lufrano, P. Staiti, M. Minutoli. *J. Electrochem. Soc.*, 2004, **151**, A64.
25 D. Ghosh, S. Giri, A. Mandal, C.K. Das, *Appl. Surf. Sci.,* 2013, **276**, 120.
26 D. Ghosh, S. Giri, A. Mandal, C.K. Das, *RSC Adv.,* 2013, **3**, 11676-11685
27 R. Ruffo, C. Wessells, R. A. Huggins, Y. Cui, *Electrochem.Commun.* 2009, **11**, 247.
28 H. Xia, Y. S. Meng, G. Yuan, C. Cui, L. Lu, *Electrochem. Solid-State Lett.* 2012**, 15**, A60.
29 A. Nakayama, A. Tanaka, Y. Sato, T. Tonosaki, K. Ogura, *Langmuir* 2005, **21**, 5907.
30 L. Niu, Z. Li, Y. Xu, J. Sun, W. Hong, X. Liu, J. Wang, S. Yang, *ACS Appl. Mater. Interfaces,* 2013, **5**, 8044.
31 X. Lang, A. Hirata, T. Fujita and M. Chen, *Nat. Nanotechnol.*, 2011, **6,** 232.
32 S. Maiti and B. B. Khatua, *RSC Adv.***,** 2013, **3**, 12874.
33 D. Ghosh, S. Giri, C. K. Das, *Nanoscale,* 2013, **5,** 10428.
34 S. Bose, T. Kuila, M. E. Uddin, N. H. Kim, A.K.T. Lau, J.H. Lee, *Polymer,* 2010, **51**, 5921.
35 G. Yu, L. Hu, N. Liu, H. Wang, M. Vosgueritchian, Y. Yang, Y. Cui, Z. Bao, *Nano Lett.* 2011, **11**, 4438.

α $MnMoO_4$/Graphene Hybrid Composite: High Energy Density Supercapacitor Electrode Material

Debasis Ghosh,[1] Soumen Giri,[1] Md. Moniruzzaman,[2] Tanya Basu,[2] Manas Mandal,[1] Chapal Kumar Das[1]*

Table of Content

Hydrothermal procedure was employed to synthesize hexahedron shaped $MnMoO_4$ wrapped with graphene exhibiting high energy density and high power density.